HMG Advance Access published July 3, 2014

Human Molecular Genetics, 2014 **1–9**
doi:10.1093/hmg/ddu323

Peripherin-2 couples rhodopsin to the CNG channel in outer segments of rod photoreceptors

Elvir Becirovic[1,2,†], O.N. Phuong Nguyen[1,2,†], Christos Paparizos[1,2], Elisabeth S. Butz[1,2], Gabi Stern-Schneider[3], Uwe Wolfrum[3], Stefanie M. Hauck[4], Marius Ueffing[4,5], Christian Wahl-Schott[1,2], Stylianos Michalakis[1,2] and Martin Biel[1,2,*]

[1]Munich Center for Integrated Protein Science CIPSM and [2]Department of Pharmacy, Center for Drug Research, Ludwig-Maximilians-Universität München, München, Germany, [3]Cell and Matrix Biology, Institute of Zoology, Johannes-Gutenberg Universität Mainz, Mainz, Germany, [4]Research Unit Protein Science, Helmholtz Center Munich, German Research Center for Environmental Health GmbH, München, Germany and [5]Center for Ophthalmology, Institute for Ophthalmic Research, Tübingen, Germany

Received May 5, 2014; Revised and Accepted June 19, 2014

Outer segments (OSs) of rod photoreceptors are cellular compartments specialized in the conversion of light into electrical signals. This process relies on the light-triggered change in the intracellular levels of cyclic guanosine monophosphate, which in turn controls the activity of cyclic nucleotide-gated (CNG) channels in the rod OS plasma membrane. The rod CNG channel is a macromolecular complex that in its core harbors the ion-conducting CNGA1 and CNGB1a subunits. To identify additional proteins of the complex that interact with the CNGB1a core subunit, we applied affinity purification of mouse retinal proteins followed by mass spectrometry. In combination with *in vitro* and *in vivo* co-immunoprecipitation and fluorescence resonance energy transfer (FRET), we found that the tetraspanin peripherin-2 links CNGB1a to the light-detector rhodopsin. Using immunoelectron microscopy, we found that this peripherin-2/rhodopsin/CNG channel complex localizes to the contact region between the disk rims and the plasma membrane. FRET measurements revealed that the fourth transmembrane domain (TM4) of peripherin-2 is required for the interaction with rhodopsin. Quantitatively, the binding affinity of the peripherin-2/rhodopsin interaction was in a similar range as that observed for rhodopsin dimers. Finally, we demonstrate that the p.G266D retinitis pigmentosa mutation found within TM4 selectively abolishes the binding of peripherin-2 to rhodopsin. This finding suggests that the specific disruption of the rhodopsin/peripherin-2 interaction in the p.G266D mutant might contribute to the pathophysiology in affected persons.

INTRODUCTION

Outer segments (OSs) of rod photoreceptors harbor all essential proteins of the phototransduction cascade including the G-protein-coupled receptor rhodopsin, the guanylyl cyclase, the phosphodiesterase and the rod cyclic nucleotide-gated (CNG) channel. Most of these proteins localize to highly structured intracellular membrane stacks (disks), which are physically separated from the plasma membrane (1). One exception is the CNG channel, which is exclusively found in the plasma membrane (2). Moreover, the periphery of disks facing the plasma membrane, referred to as disk rims, contains a set of proteins that differ from that of the remaining part of the disks. Previous studies revealed that the rod CNG channel is directly connected to the disk rims via a direct protein–protein interaction of the glutamic acid-rich (GARP) domain of the CNGB1a subunit and the disk rim-specific tetraspanin peripherin-2 (3,4). Peripherin-2 is a scaffolding protein reported to be responsible for the disk morphogenesis and for membrane fusion processes (5,6). Mutations in peripherin-2 are associated with severe retinal diseases (http://www.retina-international.org last accessed 26 June 2014). The vast majority of these mutations are linked to autosomal dominant retinitis pigmentosa (adRP), a degenerative retinal disease that affects rod photoreceptors and often results

*To whom correspondence should be addressed at: Department Pharmazie, Pharmakologie für Naturwissenschaften, Ludwig-Maximilians-Universität München, Butenandtstr. 5–13, D-81377 München, Germany. Tel: +49 89218077327; Fax: +49 89218077326; Email: mbiel@cup.uni-muenchen.de
† E.B. and O.N.P.N. contributed equally to this study.

in complete blindness. Here, we combined *in vivo* and *in vitro* biochemical, imaging and immunoaffinity methods to show that peripherin-2 in rod OSs binds to rhodopsin and the CNGB1a subunit of the CNG channel. Moreover, we demonstrate that the fourth transmembrane domain (TM4) of peripherin-2 is essential for its interaction with rhodopsin and that a single adRP-associated point mutation in TM4 of peripherin-2 abolishes this interaction while leaving the binding to CNGB1a unaffected. These results indicate that peripherin-2 operates as an adaptor protein in the disk rims that physically couples the rod CNG channel to the phototransduction cascade. This physical coupling between rhodopsin and the CNG channel suggests that phototransduction in rod OS is more spatially confined than it has been known so far and could help to gain new insights on the functional and structural role of the disk rim microcompartment in the rod OS. Finally, we conclude that the adRP phenotype in patients carrying a mutation in TM4 of peripherin-2 most probably results from the specific disruption of the peripherin-2/rhodopsin interaction in the disk rims.

RESULTS

Identification of CNGB1a-interacting proteins

To identify novel components of the rod photoreceptor, CNG channel complex of retinal lysates of light-adapted 6-week-old-mice were immunopurified using an antibody directed against the C-terminus of the CNGB1a subunit of the rod CNG channel and analyzed by quantitative mass spectrometry. Lysates of age-matched, CNGB1-deficient mice served as negative control. Among the list of OS-specific CNGB1a-interacting proteins, we identified rhodopsin and peripherin-2 (Supplementary Material, Table S1). Reciprocal co-immunoprecipitations (co-IPs) from retinal lysates using either an anti-rhodopsin antibody (Fig. 1A) or an anti-CNGB1a antibody (Fig. 1B) confirmed that rhodopsin, peripherin-2 and CNGB1a are present in the same channel complex. Importantly, no specific bands were observed when performing the co-IPs with retinal lysates from CNGB1-knockout mice (Fig. 1B, lane 2) or when a control IgG was used instead of the anti-CNGB1a antibody (Fig. 1A, lane 2). In addition to monomeric rhodopsin, the anti-rhodopsin antibody detected bands corresponding to rhodopsin oligomers (i.e. dimers, trimers and tetramers) pointing to a very tight interaction between rhodopsin molecules, which persisted under SDS–PAGE conditions. To get a more direct view on the localization of rhodopsin and CNGB1a in rod OSs, we employed immunoelectron microscopy in retinal sections (Fig. 1C). Immunogold particles of different diameters co-labeled with the anti-rhodopsin and anti-CNGB1a antibodies, respectively, revealed that CNGB1a is localized in close proximity to rhodopsin.

Analysis of the rod opsin/peripherin-2/CNGB1a complex in HEK293 cells

In previous studies, it was shown that peripherin-2 binds to the N-terminal GARP domain of CNGB1a (3,4). However, an interaction between peripherin-2 and rhodopsin or between rhodopsin and CNGB1a has not been reported so far. To address this issue, we performed co-IPs in HEK293 cells expressing different combinations of the chromophore-free rod apo-opsin (herein referred to as rod opsin), peripherin-2 and the rod CNG channel subunits (Fig. 2A and B). Surprisingly, in the absence of peripherin-2, rod opsin did not assemble with CNGB1a nor did it interact with this subunit when both subunits of the native CNG channel (CNGB1a + CNGA1) were present (Fig. 2A). In contrast, when peripherin-2 was co-expressed together with rod opsin and CNGB1a, the CNGB1a subunit could be co-immunoprecipitated with the anti-rhodopsin antibody (Fig. 2B). Moreover, peripherin-2 was binding to rod opsin in the absence of CNGB1a (Fig. 2B). Taken together, the co-IP experiments indicate that rod opsin requires peripherin-2 to interact with CNGB1a. We therefore postulated that peripherin-2 physically links rod opsin and CNGB1a by simultaneously binding to both proteins.

To test this hypothesis, we applied fluorescence resonance energy transfer (FRET) that allows detection and quantification of protein–protein interactions (Fig. 2C). We tagged the proteins C-terminally with either citrine or cerulean and then used the respective fusion protein pairs for FRET measurements. In agreement with the immunoprecipitation data, we obtained robust FRET signals for rod opsin/peripherin-2 and as well as for peripherin-2/CNGB1a. Quantitatively, FRET ratios (FRs) of these pairs were in a similar range. However, they were somewhat lower than FRs obtained for rod opsin or peripherin-2 homodimers (see also Fig. 1A and B). In agreement with previous findings (3,4), our FRET data also revealed a robust interaction between peripherin-2 and the soluble GARP2, which corresponds to the N-terminal portion of CNGB1a. Importantly, the FR obtained for the rhodopsin/CNGB1a FRET pair was only slightly above background confirming that there is no specific interaction between these two proteins.

In vitro FRET unveils binding characteristics of rod opsin and peripherin-2

To narrow down the region in peripherin-2 that is required for the interaction with rod opsin, we determined the FRs between the cerulean-tagged rod opsin and citrine-tagged peripherin-2 harboring C-terminal truncations (Fig. 3A). While deletion of the C-terminus downstream of the fourth transmembrane segment (Prph2_C1-citr) had no effect on the interaction with rod opsin, additional truncation of the TM4 domain (citr-Prph2_C2) abolished binding to rod opsin (Fig. 3A). In the latter truncation mutant (containing only three transmembrane segments), citrine was fused to the N-terminus to ensure that (like in C-terminally tagged peripherin-2 variants containing four transmembrane domains) citrine faces the cytoplasmic side of the cell. Importantly, the position of the tag did not interfere with the principal interaction with rod opsin because FRs of the peripherin-2/rod opsin pairs were in a comparable range for either N- or C-terminally tagged peripherin-2 (Fig. 3A).

In order to specifically examine protein interactions in the plasma membrane and to determine binding curves of the rod opsin/peripherin-2 interaction, confocal FRET experiments were performed in HEK293 cells (Fig. 3B and C). Maximal FR values (FR_{max}) obtained with this approach for rod opsin/peripherin-2 and rod opsin/rod opsin pairs, respectively, were in good agreement with the FR obtained in standard (non-confocal) FRET (Fig. 3A). As expected, confocal FR_{max} values were consistently higher than the corresponding

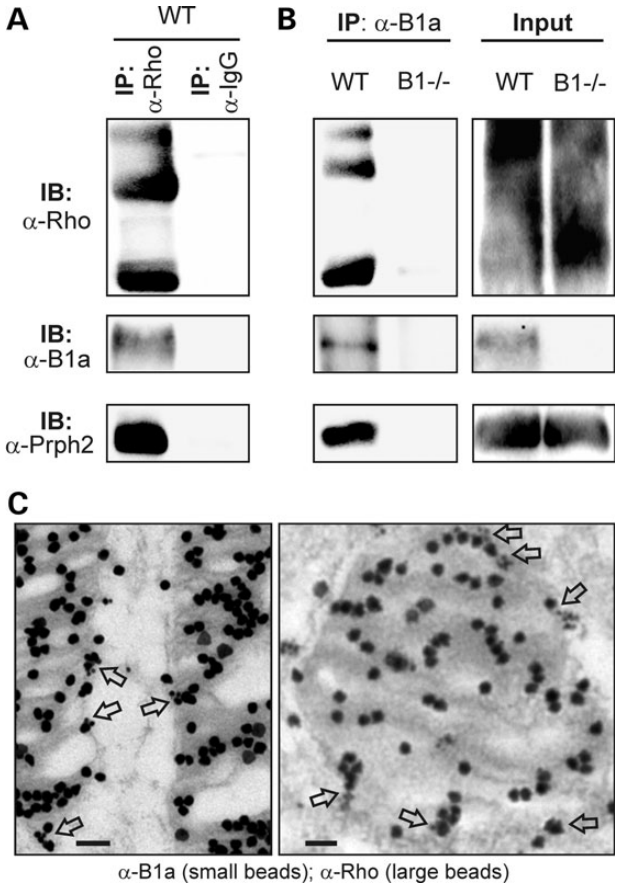

Figure 1. CNGB1a, peripherin-2 and rhodopsin are assembled in a protein complex in rod OS. (**A**) Retinal lysates of wild-type (WT) mice were immunoprecipitated with an anti-rhodopsin antibody (α-Rho) or a nonspecific control IgG (α-IgG). Precipitated samples were analyzed in immunoblots (IB) using α-Rho and antibodies directed against the CNGB1a subunit (α-B1a) and peripherin-2 (α-Prph2) as indicated. (**B**) *Left,* retinal lysates of WT and CNGB1-knockout mice (B1−/−) were immunoprecipitated with α-B1a and probed with α-Rho, α-B1a and α-Prph2. *Right*, loading control containing 10% of the protein lysate used for the co-IP in the left panel. (**C**) Immunoelectron microscopy images of longitudinal (left) and transversal (right) sections of rod OS co-stained with small-diameter immunogold particles coupled to α-B1a and large-diameter particles coupled to α-Rho, respectively. Co-localization of large and small particles is marked by arrows. Scale bar, 100 nm.

non-confocal FRs. On the basis of confocal FRET measurements, the relative binding affinity of the rod opsin/peripherin-2 interaction was calculated to be ∼80% of the rod opsin/rod opsin interaction.

FRET measurements in isolated rod OSs

To demonstrate that rhodopsin is bound to peripherin-2 in native rod photoreceptors, FRET constructs were expressed in the murine retina using AAV8-vectors, which contain the human rhodopsin promoter (Fig. 4A).Three to four weeks after subretinal injection of viral vectors, robust expression of individual constructs was observed (Fig. 4B). The expression was restricted to rod OSs indicating that the fluorophores did not interfere with the ciliary transport (Fig. 4B). OSs isolated using a self-designed quick protocol appeared to be intact with regard to their structure and shape (Fig. 4C). Figure 4D shows co-expression of a representative FRET pair (rhodopsin-cerulean and peripherin-citrin) in an isolated rod OS. As expected for a native system, FRs were throughout smaller as found upon heterologous expression in HEK293 cells (Fig. 4E). This difference most probably can be ascribed to the fact that the unlabeled wild-type proteins *in vivo* interfere with the FRET constructs leading to the reduction of the absolute FRET signal. Qualitatively, however, results in rod OSs were consistent with the results in HEK293 cells. Highest FRs were observed for the rhodopsin homomer. Importantly, there was also clear FRET between rhodopsin and peripherin-2 with the FR being slightly higher for the N-terminally as compared with the C-terminally tagged peripherin-2. In contrast, in good agreement with previous studies (4,7), no FRET was observed for rhodopsin and rod-specific GARP2 protein.

An adRP-linked mutation in TM4 of peripherin-2 disrupts binding to rhodopsin

As mentioned before, mutations in peripherin-2 have been associated with adRP. Thus, we were wondering whether some of these mutations may lead to an impaired rhodopsin binding. To address this issue, we analyzed whether some adRP-linked mutations are localized in TM4 of peripherin-2, the domain that we found to be crucial for binding to rhodopsin (cf. Fig. 3A). Indeed, one adRP-associated mutation (p.G266D) (8) was found in TM4 and was located in the transmembrane region most proximal to the intradiskal portion of peripherin-2 (Fig. 5A). Consequently, we tested whether this mutation interferes with the binding of peripherin-2 to rhodopsin. Using FRET (Fig. 5B) and co-IP (Fig. 5C) experiments from HEK293 cells, we demonstrate that the p.G266D mutant abolishes binding to rod opsin. To further demonstrate the specificity of this finding, we analyzed the effects of two additional peripherin-2 mutations on rhodopsin binding. Interestingly, the exchange of the glycine residue at position 266 and glutamate at position 276 by the neutral amino acid alanine (p.G266A and p.E276A, respectively) did not affect the binding to rhodopsin (Fig. 5B and C). Importantly, the interaction of single peripherin-2 mutants with CNGB1a was not affected as shown by additional co-IP experiments from HEK293 cells (Fig. 5D). This indicates that the lack of binding of the p.G266D mutant most probably is not due to its overall folding deficiency. Notably, for co-IP experiments, we used membrane preparations, and in the respective input controls, we could not observe any difference in the membrane expression levels of the mutants compared with the wild-type peripherin-2 (Fig. 5C and D, input controls), which argues against the lack of the membrane expression or transport deficits for any of the mutants analyzed.

DISCUSSION

In this study, we show that peripherin-2 forms a stable protein complex with both rhodopsin and the rod CNG channel in rod OS. Several lines of evidence support this conclusion. First, antibodies specific for the rod CNGB1a subunit immunoprecipitated rhodopsin from murine retinal lysates. Similarly, immunoprecipation with rhodopsin-specific antibodies pulled down CNGB1a. In both sets of experiments, peripherin-2 was

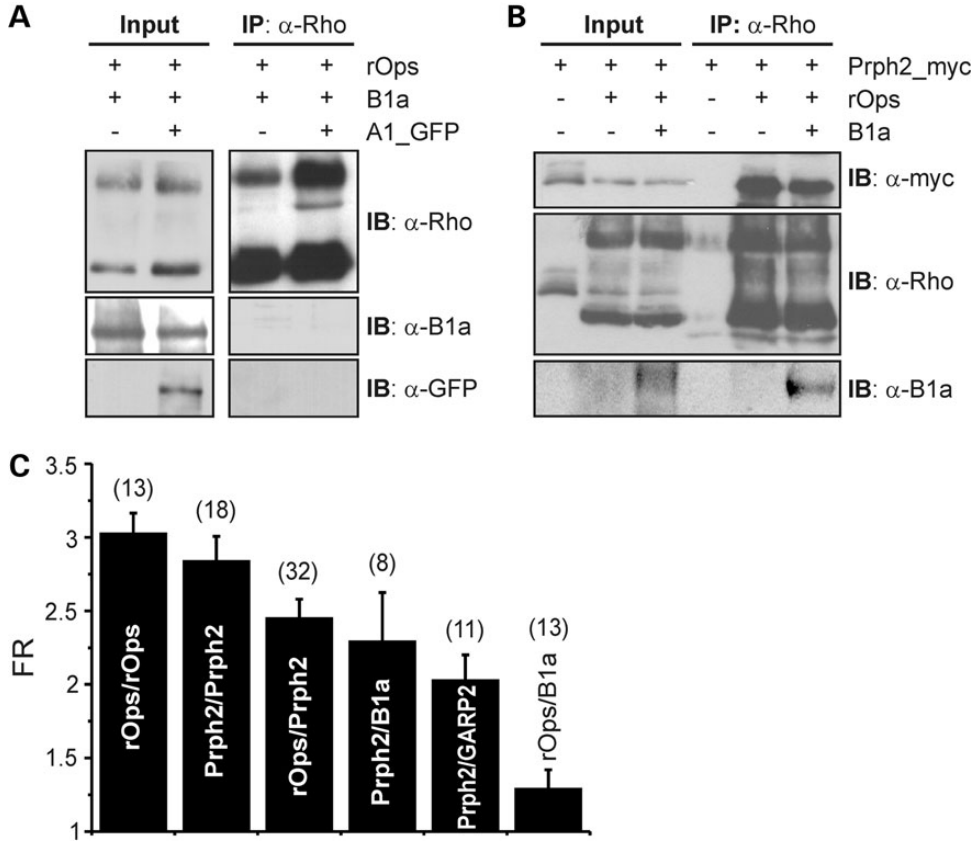

Figure 2. Peripherin-2 binds to both rod apo-opsin and CNGB1a. (**A**) Lysates from HEK293 cells co-transfected with rod apo-opsin (rOps), CNGB1a (B1a) and GFP-tagged CNGA1 (A1_GFP) were immunoprecipitated with α-Rho and probed with antibodies as indicated. (**B**) Co-IP from HEK293 cells co-expressing myc-tagged Prph2, rOps and B1a as indicated. Immunoprecipitates were analyzed with α-myc, α-Rho and α-B1a antibodies. Single transfection of peripherin-2 served as negative control for nonspecific binding to the beads (third lane from right). (**C**) FRET measurements from HEK293 cells co-transfected with different OS-specific proteins to monitor homomeric and heteromeric protein–protein interactions. Fret ratios for the single FRET pairs are as follows: rOps/rOps, FR = 3.03 ± 0.14; Prph2/Prph2, FR = 2.84 ± 0.17; rOps/Prph2, FR = 2.45 ± 0.13; Prph2/B1a, FR = 2.30 ± 0.33; Prph2/GARP2, FR = 2.03 ± 0.17; rOps/B1a, FR = 1.29 ± 0.13. Numbers of independent measurements (*n*) are given in brackets.

identified in the immunoprecipitated complex. Experiments in HEK293 cells revealed that rhodopsin does not directly bind to the CNG channel but rather requires peripherin-2 as a molecular linker to form a complex with the channel. FRET experiments strongly supported this 'bridging' function of peripherin-2. Based on our confocal FRET measurements, the relative binding affinity for the peripherin-2/rhodopsin interaction was in the similar range as for the rhodopsin/rhodopsin homomer. To the best of our knowledge, the absolute binding affinity of rhodopsin homomers was not determined so far. However, in our co-IP experiments, rhodopsin dimers and oligomers could be detected even under stringent SDS–PAGE and reducing conditions. Based on this, we expect the absolute binding affinity of rhodopsin homomers to be rather high. These results indicate that rhodopsin binds to peripherin-2 with a high affinity that is comparable with that of the rhodopsin homomer. Our biochemical and FRET experiments in isolated OSs strongly support the presence of rhodopsin dimers and oligomers in the native tissue. This is in line with recent studies providing strong evidence for the existence of rhodopsin dimers and oligomers in the native environment (9–11). In this study, we also identified the molecular determinants required for the rhodopsin/peripherin-2 interaction. As the major portion of both proteins is residing in the disk membrane of rod OS, it seems reasonable to assume that the interaction occurs via the transmembrane helices. In support of such a model, deletion of transmembrane domain 4 in peripherin-2 abolished binding to rhodopsin. Moreover, a single glycine to aspartate exchange at the position 266 in the TM4 of peripherin-2 that was previously reported in patients suffering from adRP (8) resulted in loss of binding to rhodopsin. Importantly, binding to CNGB1a was unaffected in the G266D mutant suggesting that the pathophysiological impact of this mutation relies on the impairment of the interaction with rhodopsin. The functional role of intradiskal and intracellular domains of peripherin-2 was examined in numerous studies (12). However, to our best knowledge, only one study addressed the role of a transmembrane domain of this protein showing that the glutamate residue at position 276 in TM4 was crucial for disk morphogenesis (13). Interestingly, the exchange of this charged amino acid to alanine (E276A) did not affect the interaction with rhodopsin. Similarly, the G266A mutation also had no effects on the peripherin-2/rhodopsin complex formation. These results suggest that introduction of charged residues on position 266 disrupts the binding of peripherin-2 to rhodopsin

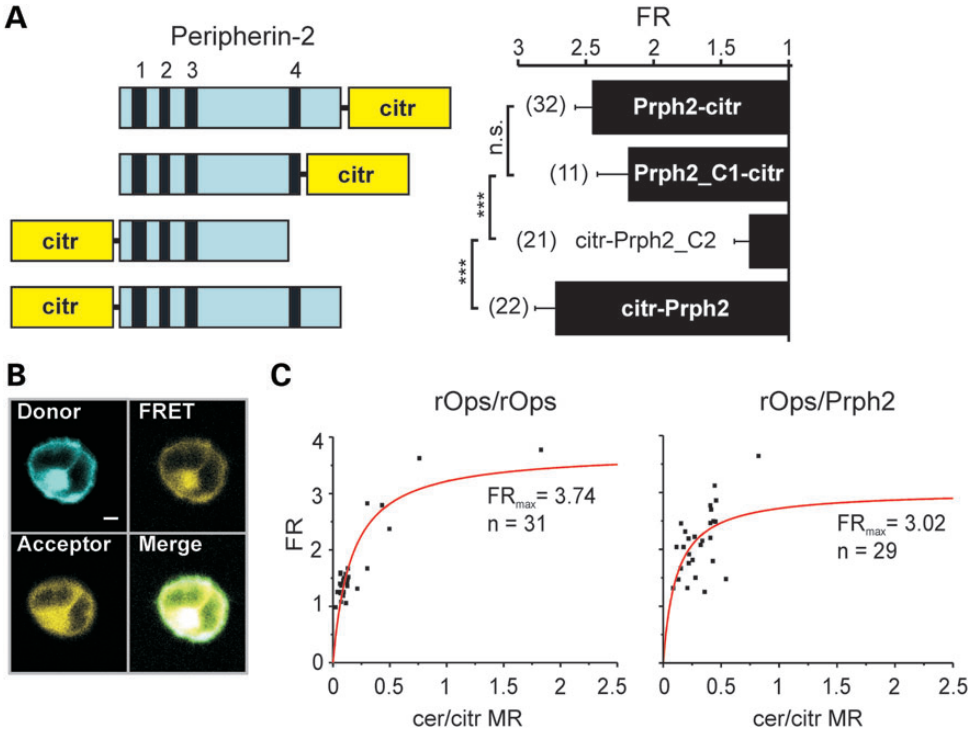

Figure 3. FRET-based determination of the binding characteristics of the rod opsin/peripherin-2 interaction. (**A**) *Left*, schematic representation of peripherin-2 constructs used to determine the FRs shown in the right panel. Citrine was fused to either the N- or C-terminus of peripherin-2. Numbered black boxes (1–4) represent the transmembrane domains of peripherin-2. *Right*, FR of the peripherin-2 constructs co-expressed with rOps-cerulean. Numbers of independent measurements (*n*) are given in brackets. Fret ratios for the single FRET pairs are as follows: rOps/Prph2-citr, FR = 2.45 ± 0.13; rOps/Prph2_C1-citr, FR = 2.19 ± 0.23; rOps/citr-Prph2_C2, FR = 1.29 ± 0.11; rOps/citr-Prph2, FR = 2.73 ± 0.15. (**B**) Representative confocal images of FRET channels (Donor, FRET, Acceptor and Merge) of single HEK293 cells used for the calculation of the FRs are shown in **C**. Scale bar = 3 μm. (**C**) Results of the confocal FRET imaging obtained from measurements of plasma membrane-restricted regions of single cells (black squares). FR was plotted against the cerulean/citrine molar ratio (cer/citr MR) to obtain FR_{max} and the binding curves.

whereas neutral amino acids at the same position do not affect this interaction. Taken together, our data point to a key role of TM4 for the peripherin-2/rhodopsin interaction and suggest that impaired binding to rhodopsin may contribute to the pathophysiology of peripherin-2 mutations.

As is evident in Figure 5C and D, two bands for wild-type peripherin-2 are detected in the inputs and co-IP experiments. The upper band of peripherin-2 is most likely not a result of glycosylation because our protein samples were deglycosylated prior to the SDS–PAGE. Intriguingly, the relative intensities of the two bands correlate with the number of negative charges in TM4. In the G266D mutant that contains two negative charges (E276 and D266), the upper band is stronger than the lower band. In contrast, in G266A and wild type containing one negative charge in TM4 (E276), the lower band is stronger than the upper band. Finally, in the E276A mutant containing no negative charge, only the lower band is visible. A potential effect of charges on the conformation and relative mobility of peripherin-2 would be in agreement with previous findings showing that single mutants can lead to a differential electrophoretic mobility of the corresponding protein (14).

Finally, we used FRET and immunoelectron microscopy to directly demonstrate that rhodopsin and CNGB1a are located in close proximity in rod OS. Overall, our results are consistent with the model shown in Figure 6. The novel aspect of this model is that peripherin-2 by binding to both, rhodopsin and the CNG channel, physically couples the most proximal protein of the light transduction cascade (rhodopsin) with the most distal protein (the CNG channel) in a narrow spatial microcompartment encompassing the disk rims and the neighboring plasma membrane. One could imagine two principal scenarios where the supramolecular organization of these proteins might be relevant. First, the complex could play a structural role in the formation and maintenance of rod OS structure. Mutations in peripherin-2 as well as in rhodopsin are associated with impaired disk morphogenesis and stability resulting in shortened and deteriorated rod OS (15–18). Structural impairments of OS are also seen upon mutation of ROM1, another photoreceptor-specific protein that binds to peripherin-2 (19), and in CNGB1a-knockout mice lacking the peripherin-2-binding GARP domain (20). Taken together, these findings imply that the integrity of the rhodopsin/peripherin-2/ROM1/CNG channel complex is crucial for morphogenesis and long-term stability of rod OS. Loss or functional impairment of any of the constituents of the complex will thus lead to more or less severe structural defects. In support to a structural role of the rhodopsin/peripherin-2 interaction, the addition of rhodopsin to the reconstituted peripherin-2/ROM1 complex in lipid vesicles was recently reported to induce the formation of disk rim-like structures *in vitro* (21).

The second scenario refers to a functional role of the complex in visual transduction. By binding to both, rhodopsin and the CNG channel, peripherin-2 helps to generate a microcompartment in

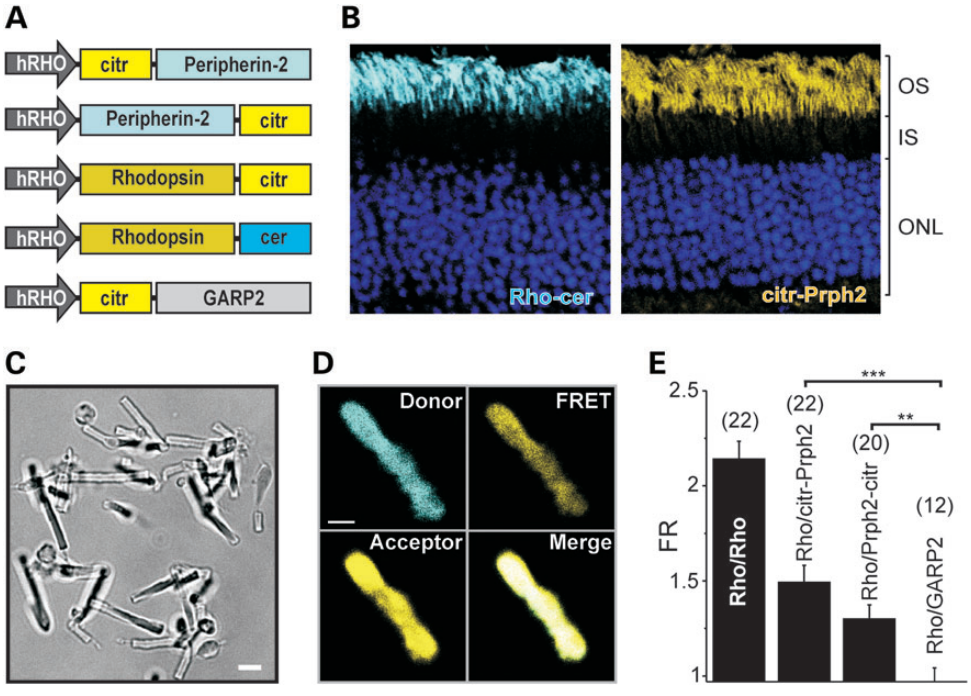

Figure 4. FRET in isolated rod OS from WT mice injected with different rAAV constructs. (**A**) Schematic view of the constructs used for the rAAV-mediated transduction of retinas from P14 C57/Bl6N WT mice. hRHO, human rhodopsin promoter. (**B**) Representative confocal images of retinal sections from mice expressing rhodopsin-cerulean (left) and citrin-peripherin-2 (right). OS, outer segment; IS, inner segment; ONL, outer nuclear layer. (**C**) Bright-field images of an isolated OS isolated from mouse retina. (**D**) Representative confocal image of a single OS used for FRET measurements and co-expressing rhodopsin-cerulean (donor) and peripherin-2-citrin (acceptor), respectively. Scale bar = 2 μm. (**E**) Results of the FRET measurements for different FRET pair combinations. Numbers of independent measurements (*n*) are given in brackets. FRET ratios for the single FRET pairs are as follows: Rho/Rho, FR = 2.14 ± 0.09; Rho/citr-Prph2, FR = 1.49 ± 0.09; Rho/Prph2-citr, FR = 1.30 ± 0.07; Rho/GARP2, FR = 0.97 ± 0.07.

the rim disk region that could have evolved to optimize the sensitivity and precision of light transduction. Recently, it was reported that a substantial portion of the rod phosphodiesterase (PDE6) is located at the disk rims of rod OS (22). GARP2 that was shown to bind PDE6, peripherin-2, and the CNG channel subunits (3,23,24) could serve as an adaptor protein that anchors PDE6 to the disk rim. Another study also reported a physical interaction of PDE6 and the rod CNG channel (25). The proposed complex would be exquisitely efficient because the distance between the light harvesting rhodopsin, the guanosine monophosphate (cGMP)-hydrolyzing PDE6 and the channel that translates changes in cGMP in changes of the Na^+/Ca^{2+} flux would be extremely short. In contrast to rhodopsin, the CNG channel and peripherin-2 were reported to be absent in the central disk region (2,26,27). Consequently, in this region, rhodopsin is physically uncoupled from the CNG channel. At the moment, only one can speculate about the exact functional role of the differential microcompartmentalization of rhodopsin in the central and peripheral part of the disks. Owing to the shorter diffusion distance for cGMP, however, the disk rim-associated complex is expected to operate at lower light intensities and faster kinetics. Such an optimization could be important in rods, which are tailored to detect extremely low light levels. In contrast, in the less light-sensitive cones, coupling of the light sensor to the channel seems less important. In agreement with this hypothesis, the cone CNG channel subunits lack the GARP domain that is required for the interaction with peripherin-2 (3,28,29).

MATERIALS AND METHODS

Animals

All procedures concerning animals were performed with permission of local authorities (Regierung von Oberbayern).

Molecular biology

Full-length CNGB1a, GARP2, peripherin-2 and rhodopsin were PCR-amplified from mouse retinal cDNA and subcloned into the pcDNA3.1Myc/His expression vector (Invitrogen). For FRET measurements and for *in vitro* co-IP studies, the FRET-optimized YFP and CFP derivatives citrine or cerulean (30–32) were introduced N- or C-terminally to the respective constructs by standard cloning procedures. Peripherin-2 deletion mutations were obtained by site-directed mutagenesis (QuikChange Lightning Mutagenesis Kit, Agilent Technologies) and overlap PCR techniques. All constructs amplified by PCR were completely sequenced prior to use. For the FRET studies on rod OS, the appropriate FRET constructs were subcloned to the previously described single-stranded pAAV2.1 vector (33) containing a human rhodopsin (hRHO) promoter.

Retina preparation and protein biochemistry

For *in vivo* co-IPs and for quantitative mass spectrometry, freshly dissected retinas were homogenized in 1% Triton X-100 solution under normal daylight illumination, which

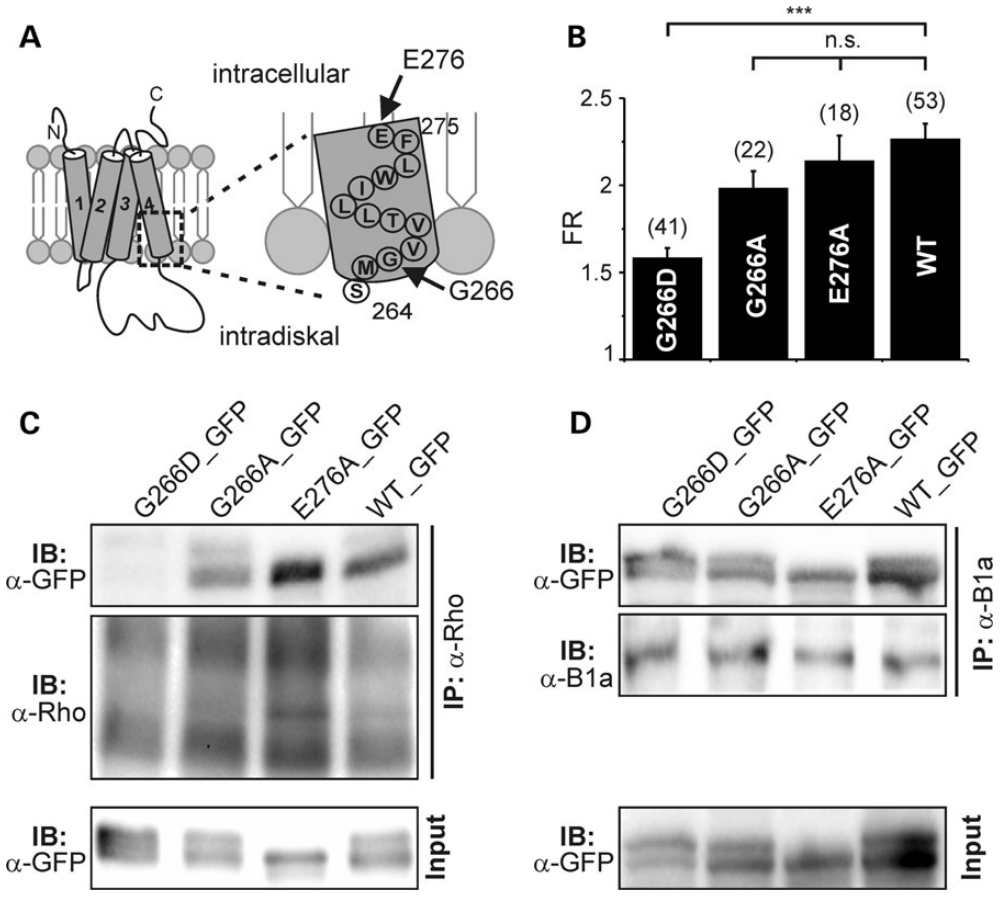

Figure 5. adRP-associated mutation in TM4 of peripherin-2 abolishes binding to rhodopsin. (**A**) Schematic view of the positions of the mutations in the TM4 of peripherin-2 analyzed in **B**–**C** (black arrows). (**B**) FRET experiment from HEK293 cells co-transfected with rod opsin and peripherin-2 wild-type (WT) or mutant constructs, respectively. FRET ratios for the single FRET pairs are as follows: Rho/G266D, FR = 1.58 ± 0.05; Rho/G266A, FR = 1.98 ± 0.09; Rho/E276A, FR = 2.14 ± 0.14; Rho/WT, FR = 2.26 ± 0.08. (**C**) Co-IP from HEK293 cells co-expressing rhodopsin and GFP-tagged wild-type or mutant peripherin-2 constructs. (**D**) Co-IP from HEK293 cells co-expressing CNGB1a and GFP-tagged wild-type or mutant peripherin-2 constructs. All peripherin-2 constructs in C and D were detected with the GFP-specific antibody (α-GFP).

results in bleached rhodopsin. Subsequently, cell debris was removed by 5000 × *g* centrifugation for 15 min, and protein concentration of the supernatant was determined by Bradford. For mass spectrometry, 50 µl of the magnetic beads (Dynabeads® Protein A, Invitrogen) were pre-incubated with 5 µg of the CNGB1 antibody (34) in a total volume of 500 µl of PBS for 2 h at 4°C. After the removal of PBS, the pre-coupled beads were incubated over night at 4°C with 500 µg of total retinal protein per single reaction. Next steps were performed according to manufacturer's instructions. After the removal of magnetic beads, the immunoaffinity purified proteins were analyzed via LC MS/MS as described previously (35).

For *in vivo* co-IP experiments, anti-B1a, anti-rhodopsin [mouse anti-Rho 1D4, Thermo Scientific) and anti-peripherin-2 (mouse anti-Prph2 2B7 (36)] antibodies were used followed by the same protocol as described earlier for the mass spectrometry. The anti-B1a antibody recognizes the distal C-terminus of the rod-specific CNGB1a and the olfactory-specific CNGB1b subunit (34). Immunopurified proteins were separated on a 6–12% SDS–PAGE gradient gel and proceeded for western blotting. Antibodies were used in the following dilutions: rabbit anti-B1a, 1 : 1000; mouse anti-Prph2, 1 : 1000; mouse anti-Rho, 1 : 2000; mouse anti-myc, 1 : 2000 (Cell Signaling); mouse anti-GFP (Clontech), 1 : 2000. *In vitro* co-IPs were performed as described previously (23). Rod opsin signals from untreated HEK293 protein lysates are detected as a smear on western blot owing to an extensive rod opsin glycosylation. Hence, prior to the sample loading to the SDS–PAGE gel, a deglycosylation step was included using PNGase F (New England Biolabs) according to the instructions of the manufacturer. For *in vitro* co-IPs with the anti-myc or anti-GFP antibody, the µMACS GFP or myc-tagged beads were used (Miltenyi Biotec). All steps were performed in accordance with the manufacturer's protocol.

Photometric FRET measurements

Digital FRET measurements were performed as described (37). For confocal FRET measurements, HEK293 cells were grown in 5-cm cell culture dishes (Greiner bio-one) and transiently transfected using the calcium phosphate method. After 24–48 h, the cells were washed and maintained in buffer solution composed of 140 mM NaCl, 5 mM KCl, 1 mM $MgCl_2$, 2 mM $CaCl_2$, 10 mM glucose, 10 mM Na-HEPES, pH 7.4, at room temperature.

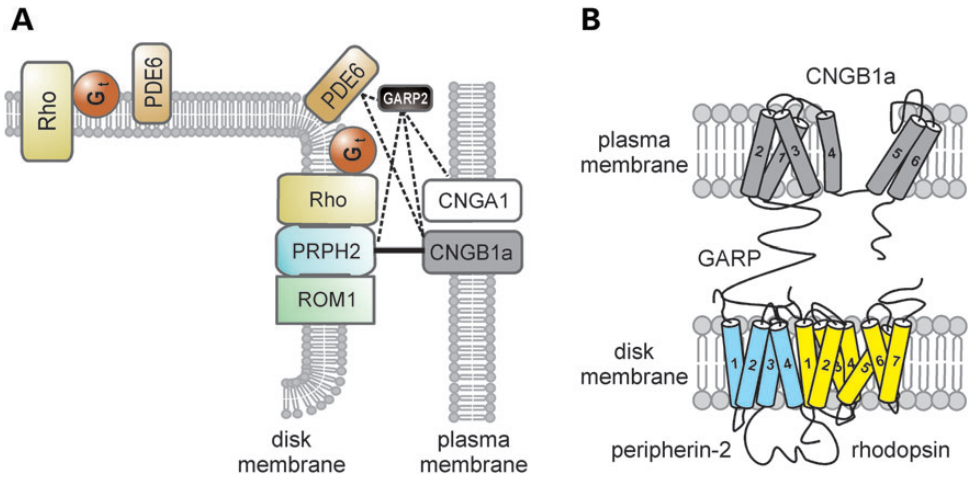

Figure 6. Peripherin-2 couples the CNG channel to the phototransduction cascade in rod OS. (**A**) Simplified paradigm of protein–protein interactions in the disk rim region of OS. Peripherin-2 simultaneously binds to its homolog ROM1, to CNGB1a and to rhodopsin. The soluble GARP2 undergoes multiple protein–protein interactions with CNGB1a, CNGA1, phosphodiesterase (PDE6) and peripherin-2 as indicated by the dashed line. Gt, transducin. (**B**) Tentative model of the CNGB1a/peripherin-2/rhodopsin complex. Note that the exact portion of rhodopsin that binds to TM4 of peripherin-2 is not known and is only tentatively assigned in this cartoon.

Cells were imaged using a Leica TCS SP8 confocal microscope with a 20× water objective (1.0 numerical aperture). Excitation of cerulean was performed with a 448-nm laser followed by emission measurements between 483 ± 16 nm. Citrine was excited with a 514-nm laser beam, and emission was measured between 542 ± 17 nm. FRET images were obtained by 448-nm excitation and 542 ± 17-nm emission. Cerulean, FRET and citrine images were acquired simultaneously, and all images were performed under the same laser intensity, photomultiplier gain and pinhole settings. The intensities of the signals were subtracted from the background, and FRs were calculated according to the three cube FRET equations described in (37). Cell membrane was defined as region of interest, and images of cells with over- or under-saturated cerulean or citrine signals were omitted from further analysis. For the conversion of fluorescence intensities obtained from measurements in cells expressing separate cerulean- and citrine-labeled proteins into molar cer/citr ratios, we used a correction factor, $R = 3$ (37). To calculate FR_{max} and to obtain the binding curves, FRs of the respective FRET pairs were plotted versus the cer/citr ratios and fitted to a hyperbolic function: $(P1 \times X)/(P2 + X)$. X is the FRET values of the single cells and P1 and P2 were calculated by 100 iterations for each FRET pair. P1 is the limiting value of the function and equals FR_{max}. For the determination of the relative binding affinity, the following equation was used: $(FR_{max}Prph2/FR_{max}rOps) \times 100$.

Statistics

All values are given as mean ± SE, and n is the number of animals or trials. Unless stated otherwise, an unpaired student's t-test was performed for the comparison between two groups. Statistical significance is given as follows: $^{*}P < 0.05$; $^{**}P < 0.01$; $^{***}P < 0.001$. If multiple comparisons were made, significance was tested by analysis of variance followed by Dunnett's test. For analysis of the LC MS/MS data, one-way ANOVA was used.

Preparation of OSs

Single retinas were dissected and transferred to 200 µl of PBS. The OSs were mechanically separated by mixing the solution for 10–20 s on a standard shaking device. The solution was spun for few seconds to remove cell debris. The supernatant containing the OSs was transferred to cell culture dishes (ibiTreat, ibidi, Martinsried, Germany). Prior to the FRET measurements, the OSs were allowed to sediment for ∼15 min.

rAAV preparation and subretinal injections

The production of single-strand AAVs and the procedure of subretinal injections were described previously (33). A total of 10^8–10^{10} rAAV particles were delivered by a single injection.

Immunoelectron microscopy

The preparation for immunoelectron microscopy was performed as previously described (38). Labeled LRWhite ultrathin sections were analyzed in a transmission electron microscope (Tecnai 12 BioTwin; FEI, Eindhoven, The Netherlands). Images were obtained with a charge-coupled device camera (SIS Megaview3; Surface Imaging Systems), acquired by analySIS (Soft Imaging System) and processed with Adobe Photoshop CS. Antibodies used were as follows: anti-B1a, anti-Rho and anti-Prph2 (PER5H2, (39).

SUPPLEMENTARY MATERIAL

Supplementary Material is available at *HMG* online.

ACKNOWLEDGEMENTS

We thank Berit Noack for excellent technical support. We also thank Muna Naash and Robert Molday for the gift of the peripherin-2 antibody.

Conflict of Interest statement. None declared.

FUNDING

This work was supported by the Deutsche Forschungsgemeinschaft.

REFERENCES

1. Sung, C.H. and Chuang, J.Z. (2010) The cell biology of vision. *J. Cell Biol.*, **190**, 953–963.
2. Cook, N.J., Molday, L.L., Reid, D., Kaupp, U.B. and Molday, R.S. (1989) The cGMP-gated channel of bovine rod photoreceptors is localized exclusively in the plasma membrane. *J. Biol. Chem.*, **264**, 6996–6999.
3. Poetsch, A., Molday, L.L. and Molday, R.S. (2001) The cGMP-gated channel and related glutamic acid-rich proteins interact with peripherin-2 at the rim region of rod photoreceptor disc membranes. *J. Biol. Chem.*, **276**, 48009–48016.
4. Ritter, L.M., Khattree, N., Tam, B., Moritz, O.L., Schmitz, F. and Goldberg, A.F. (2011) In situ visualization of protein interactions in sensory neurons: glutamic acid-rich proteins (GARPs) play differential roles for photoreceptor outer segment scaffolding. *J. Neurosci.*, **31**, 11231–11243.
5. Boesze-Battaglia, K. and Goldberg, A.F. (2002) Photoreceptor renewal: a role for peripherin/rds. *Int. Rev. Cytol.*, **217**, 183–225.
6. Conley, S.M., Stuck, M.W. and Naash, M.I. (2012) Structural and functional relationships between photoreceptor tetraspanins and other superfamily members. *Cell Mol. Life Sci.*, **69**, 1035–1047.
7. Korschen, H.G., Beyermann, M., Muller, F., Heck, M., Vantler, M., Koch, K.W., Kellner, R., Wolfrum, U., Bode, C., Hofmann, K.P. *et al.* (1999) Interaction of glutamic-acid-rich proteins with the cGMP signalling pathway in rod photoreceptors. *Nature*, **400**, 761–766.
8. Sohocki, M.M., Daiger, S.P., Bowne, S.J., Rodriquez, J.A., Northrup, H., Heckenlively, J.R., Birch, D.G., Mintz-Hittner, H., Ruiz, R.S., Lewis, R.A. *et al.* (2001) Prevalence of mutations causing retinitis pigmentosa and other inherited retinopathies. *Hum. Mutat.*, **17**, 42–51.
9. Fotiadis, D., Liang, Y., Filipek, S., Saperstein, D.A., Engel, A. and Palczewski, K. (2003) Atomic-force microscopy: rhodopsin dimers in native disc membranes. *Nature*, **421**, 127–128.
10. Knepp, A.M., Periole, X., Marrink, S.J., Sakmar, T.P. and Huber, T. (2012) Rhodopsin forms a dimer with cytoplasmic helix 8 contacts in native membranes. *Biochemistry*, **51**, 1819–1821.
11. Suda, K., Filipek, S., Palczewski, K., Engel, A. and Fotiadis, D. (2004) The supramolecular structure of the GPCR rhodopsin in solution and native disc membranes. *Mol. Membr. Biol.*, **21**, 435–446.
12. Goldberg, A.F. (2006) Role of peripherin/rds in vertebrate photoreceptor architecture and inherited retinal degenerations. *Int. Rev. Cytol.*, **253**, 131–175.
13. Goldberg, A.F., Ritter, L.M., Khattree, N., Peachey, N.S., Fariss, R.N., Dang, L., Yu, M. and Bottrell, A.R. (2007) An intramembrane glutamic acid governs peripherin/rds function for photoreceptor disk morphogenesis. *Invest. Ophthalmol. Vis. Sci.*, **48**, 2975–2986.
14. Shi, Y., Mowery, R.A., Ashley, J., Hentz, M., Ramirez, A.J., Bilgicer, B., Slunt-Brown, H., Borchelt, D.R. and Shaw, B.F. (2012) Abnormal SDS-PAGE migration of cytosolic proteins can identify domains and mechanisms that control surfactant binding. *Protein Sci.*, **21**, 1197–1209.
15. Humphries, M.M., Rancourt, D., Farrar, G.J., Kenna, P., Hazel, M., Bush, R.A., Sieving, P.A., Sheils, D.M., McNally, N., Creighton, P. *et al.* (1997) Retinopathy induced in mice by targeted disruption of the rhodopsin gene. *Nat. Genet.*, **15**, 216–219.
16. Lem, J., Krasnoperova, N.V., Calvert, P.D., Kosaras, B., Cameron, D.A., Nicolo, M., Makino, C.L. and Sidman, R.L. (1999) Morphological, physiological, and biochemical changes in rhodopsin knockout mice. *Proc. Natl Acad. Sci. USA*, **96**, 736–741.
17. Sanyal, S. and Jansen, H.G. (1981) Absence of receptor outer segments in the retina of rds mutant mice. *Neurosci. Lett.*, **21**, 23–26.
18. Travis, G.H., Sutcliffe, J.G. and Bok, D. (1991) The retinal degeneration slow (rds) gene product is a photoreceptor disc membrane-associated glycoprotein. *Neuron*, **6**, 61–70.
19. Clarke, G., Goldberg, A.F., Vidgen, D., Collins, L., Ploder, L., Schwarz, L., Molday, L.L., Rossant, J., Szel, A., Molday, R.S. *et al.* (2000) Rom-1 is required for rod photoreceptor viability and the regulation of disk morphogenesis. *Nat. Genet.*, **25**, 67–73.
20. Zhang, Y., Molday, L.L., Molday, R.S., Sarfare, S.S., Woodruff, M.L., Fain, G.L., Kraft, T.W. and Pittler, S.J. (2009) Knockout of GARPs and the beta-subunit of the rod cGMP-gated channel disrupts disk morphogenesis and rod outer segment structural integrity. *J. Cell Sci.*, **122**, 1192–1200.
21. Kevany, B.M., Tsybovsky, Y., Campuzano, I.D., Schnier, P.D., Engel, A. and Palczewski, K. (2013) Structural and functional analysis of the native peripherin-ROM1 complex isolated from photoreceptor cells. *J. Biol. Chem.*, **288**, 36272–36284.
22. Chen, J., Yoshida, T. and Bitensky, M.W. (2008) Light-induced translocation of cyclic-GMP phosphodiesterase on rod disc membranes in rat retina. *Mol. Vis.*, **14**, 2509–2517.
23. Michalakis, S., Zong, X., Becirovic, E., Hammelmann, V., Wein, T., Wanner, K.T. and Biel, M. (2011) The glutamic acid-rich protein is a gating inhibitor of cyclic nucleotide-gated channels. *J. Neurosci.*, **31**, 133–141.
24. Pentia, D.C., Hosier, S. and Cote, R.H. (2006) The glutamic acid-rich protein-2 (GARP2) is a high affinity rod photoreceptor phosphodiesterase (PDE6)-binding protein that modulates its catalytic properties. *J. Biol. Chem.*, **281**, 5500–5505.
25. Bennett, N., Ildefonse, M., Crouzy, S., Chapron, Y. and Clerc, A. (1989) Direct activation of cGMP-dependent channels of retinal rods by the cGMP phosphodiesterase. *Proc. Natl Acad. Sci. USA*, **86**, 3634–3638.
26. Molday, R.S., Hicks, D. and Molday, L. (1987) Peripherin. A rim-specific membrane protein of rod outer segment discs. *Invest. Ophthalmol. Vis. Sci.*, **28**, 50–61.
27. Molday, R.S., Molday, L.L., Dose, A., Clark-Lewis, I., Illing, M., Cook, N.J., Eismann, E. and Kaupp, U.B. (1991) The cGMP-gated channel of the rod photoreceptor cell characterization and orientation of the amino terminus. *J. Biol. Chem.*, **266**, 21917–21922.
28. Conley, S.M., Ding, X.Q. and Naash, M.I. (2010) RDS in cones does not interact with the beta subunit of the cyclic nucleotide gated channel. *Adv. Exp. Med. Biol.*, **664**, 63–70.
29. Molday, R.S. and Molday, L.L. (1998) Molecular properties of the cGMP-gated channel of rod photoreceptors. *Vision Res.*, **38**, 1315–1323.
30. Griesbeck, O., Baird, G.S., Campbell, R.E., Zacharias, D.A. and Tsien, R.Y. (2001) Reducing the environmental sensitivity of yellow fluorescent protein mechanism and applications. *J. Biol. Chem.*, **276**, 29188–29194.
31. Rizzo, M.A., Springer, G.H., Granada, B. and Piston, D.W. (2004) An improved cyan fluorescent protein variant useful for FRET. *Nat. Biotechnol.*, **22**, 445–449.
32. Zacharias, D.A., Violin, J.D., Newton, A.C. and Tsien, R.Y. (2002) Partitioning of lipid-modified monomeric GFPs into membrane microdomains of live cells. *Science*, **296**, 913–916.
33. Koch, S., Sothilingam, V., Garcia Garrido, M., Tanimoto, N., Becirovic, E., Koch, F., Seide, C., Beck, S.C., Seeliger, M.W., Biel, M. *et al.* (2012) Gene therapy restores vision and delays degeneration in the CNGB1(−/−) mouse model of retinitis pigmentosa. *Hum. Mol. Genet.*, **21**, 4486–4496.
34. Huttl, S., Michalakis, S., Seeliger, M., Luo, D.G., Acar, N., Geiger, H., Hudl, K., Mader, R., Haverkamp, S., Moser, M. *et al.* (2005) Impaired channel targeting and retinal degeneration in mice lacking the cyclic nucleotide-gated channel subunit CNGB1. *J. Neurosci.*, **25**, 130–138.
35. Hauck, S.M., Dietter, J., Kramer, R.L., Hofmaier, F., Zipplies, J.K., Amann, B., Feuchtinger, A., Deeg, C.A. and Ueffing, M. (2010) Deciphering membrane-associated molecular processes in target tissue of autoimmune uveitis by label-free quantitative mass spectrometry. *Mol. Cell Proteomics*, **9**, 2292–2305.
36. Conley, S.M., Stricker, H.M. and Naash, M.I. (2010) Biochemical analysis of phenotypic diversity associated with mutations in codon 244 of the retinal degeneration slow gene. *Biochemistry*, **49**, 905–911.
37. Shaltiel, L., Paparizos, C., Fenske, S., Hassan, S., Gruner, C., Rotzer, K., Biel, M. and Wahl-Schott, C.A. (2012) Complex regulation of voltage-dependent activation and inactivation properties of retinal voltage-gated Cav1.4 L-type Ca2+ channels by Ca2+-binding protein 4 (CaBP4). *J. Biol. Chem.*, **287**, 36312–36321.
38. Wolfrum, U. and Schmitt, A. (2000) Rhodopsin transport in the membrane of the connecting cilium of mammalian photoreceptor cells. *Cell Motil. Cytoskeleton*, **46**, 95–107.
39. Connell, G., Bascom, R., Molday, L., Reid, D., McInnes, R.R. and Molday, R.S. (1991) Photoreceptor peripherin is the normal product of the gene responsible for retinal degeneration in the rds mouse. *Proc. Natl Acad. Sci. USA*, **88**, 723–726.